RSC Advances

PAPER

View Article Online
View Journal | View Issue

Cite this: *RSC Adv.*, 2017, **7**, 51303

Effect of PET graft coated with silk fibroin *via* EDC/NHS crosslink on graft-bone healing in ACL reconstruction

Chengchong Ai,[a] Jiangyu Cai,[a] Jun Zhu,[b] Juan Zhou,[b] Jia Jiang*[a] and Shiyi Chen*[a]

Anterior cruciate ligament (ACL) reconstruction under arthroscopy using (PET) artificial ligaments helps to return to sport earlier compared with using autografts and allografts, but defective biocompatibility of PET worries surgeons. The purpose of this study is to investigate whether silk fibroin coating on PET *via* EDC/NHS crosslink could promote the compatibility of PET and enhance graft-bone healing. SF was immobilized on the surface of PET ligaments *via* EDC/NHS crosslinking method. Changes in the surface properties were characterized by scanning electron microscope (SEM), water contact angle measurement, and Fourier transform infrared spectra (FTIR). SF coating enhanced the hydrophilia of PET. *In vitro* studies by culturing BMSCs demonstrated that SF coating could improve BMSCs proliferation and increase the expression level of BMP-2, OCN, collagen I. Rabbit ACL reconstruction model was applied to observe the graft-bone healing process *in vivo*. The histological results proved that SF coating promoted graft-bone healing. However, the histological improvement was not translated into significant amelioration in biomechanical results and micro-CT analysis. In conclusion, SF coating *via* EDC/NHS crosslink improved the graft-bone healing of PET ligaments within the bone tunnel, which might positively influence the outcome of ACL reconstruction.

Received 4th August 2017
Accepted 24th October 2017

DOI: 10.1039/c7ra08636a

rsc.li/rsc-advances

1. Introduction

The anterior cruciate ligament (ACL) is of great importance to maintain a good stability and motion function of knee, while it is also the most frequently injured ligament in the knee joint, which may result in knee instability, meniscus injury, and articular cartilage injury.[1] ACL reconstruction under arthroscopy has become the golden standard for the treatment of ACL rupture, especially for those suffering from acute injury and preserving remnants of ligament.[2] Autografts and allografts are recognized as the optimal choice in clinical, but they have been recently overtaken by artificial ligaments which can not only avoid donor site morbidity and disease transmission, but also ensure a fast recovery and quick return to sport because of its strong mechanical property.[3] Ligament Advanced Reinforcement System (LARS; Surgical Implants and Devices, ArcsuiTille, France) ligament, made of polyethylene terephthalate (PET) material, is the most commonly-used artificial graft for ACL reconstruction at present, producing satisfactory results in the reconstruction of knee ligaments.[4–6] However, there are still many failure cases as the clinical follow-up studies have observed, including synovitis, bone tunnel enlargement, and graft rupture. Especially, at the graft–bone interface interposed a layer of fibrous scar tissue,[6] which is ascribed to the lack of good biocompatibility for osseointegration in the bone tunnel.

Silk fibroin (SF) have been used as sutures for centuries clinically and receives more and more concern due to its biocompatibility, slow degradability and remarkable mechanical properties for biomaterial application including the engineering of bone, cartilage, skin, ligaments, tendons, and cardiac tissue.[7–11] A silk fibroin structure was designed to support the attachment, expansion and differentiation of cells, and its tensile force was capable of matching the mechanical requirement of ACL, which revealed its great potential for ACL repair.[12] Moreover, it was proven to be effectual to fabricate mesenchymal stem cells seeded silk scaffold for pig ACL regeneration model in which ligament–bone interface with typical four zone (*e.g.*, bone, mineralized fibrocartilage, fibrocartilage, and ligament) was observed.[13] It was proved that silk scaffolds with additional cell seeding can promote the ligament tissue regeneration in rabbit ACL reconstruction model and sheep ACL reconstruction model.[14,15] These findings revealed its potential for osseointegration and ligamentization required by graft-healing process.

However, the effect of silk scaffold is time-limited due to its biodegradation, and premature collapse of the silk structures would result in necrosis.[16] It was reported SF fibers lose the majority of their tensile strength within 1 year *in vivo* generally.[7] Afterwards, it is doubtful whether newly born tissue is strong

[a]*Department of Sports Medicine, Huashan Hospital, Fudan University, 12 Middle Wulumuqi Road, Shanghai 200040, China. E-mail: cshiyi@163.com; Jessicajj19@hotmail.com*

[b]*National Engineering Research Center for Nanotechnology, Shanghai 200241, China*

enough to bear the required tensile strength of ACL. The stability of PET ligaments can help to make up for this weakness. Besides, the good biocompatibility of SF exactly conforms to the clinical requirement for PET ligaments. Coating on graft surface is a considerable method to induce osseointegration.[17] In our previous study, SF exhibited its great potential as the modified material of PET to enhance osseointegration.[18] In order to improve the coating adherence, we utilized crosslinking method to modify PET surface in the current study. 1-Ethyl-3-(3-dimethylaminopropyl)carbodiimide (EDC) facilitates to bond carboxyl and amidogen to form an amide bond as crosslinking material; *N*-hydroxysuccinimide (NHS) contributes to improve the stability of EDC crosslinking products.[19] EDC/NHS crosslinking is frequently used to stabilize biomaterials with well-defined pore geometry especially collagen-based scaffolds for optimal cell infiltration.[20,21]

We hypothesized that SF coating *via* EDC/NHS crosslink has a positive effect in promoting the compatibility of PET thus enhancing graft-bone healing after implantation. To be specific, the current study was carried out in terms of three folds: (1) to prove the effectiveness of EDC/NHS crosslinking method for modifying PET with SF; (2) to compare the performance of bone marrow stromal cells (BMSCs) *in vitro* before and after SF coating onto PET; (3) to observe the process of graft-bone osseointegration in rabbit ACL reconstruction model. To obtain an efficient method to modify PET is significant to fabricate an ideal artificial ligament meeting the clinical needs.

2. Experimental section

2.1 SF coating preparation and immobilization on PET sheets

Silk fibroin was prepared according to established procedures.[22] *Bombyx mori* silk was degummed by means of boiling in 5 g L^{-1} Na_2CO_3 solution for 1 h. After sericin was removed, the degummed silk was dissolved in $CaCl_2/H_2O/C_2H_5OH$ ternary solvent for 40 min at 80 °C, specifically 1 g degummed silk fibroin in 10 mL ternary solvent, followed by filtering and dialyzing against deionized water with a 14 000 molecular weight cutoff dialysis membrane for 72 h at room temperature. The dialyzed solution was collected that was 3% (w/w) aqueous regenerated SF solution. Silk fibroin powder was prepared by casting the solution in freeze dryer at −80 °C.

PET sheets were dipped in absolute ethyl alcohol solution for 30 min and treated by ultrasonication for 10 min. The cleaned PET sheets were boiled in NaOH aqueous solution for 1 h to expose carboxyl and washed with a large amount of deionized water, named PET–COOH group. The SF coating through EDC–NHS crosslink was prepared.[23] Firstly, the carboxyl-exposed PET sheets were immersed in MES buffer (pH = 5.5) for 2 h. Secondly, EDC (0.1 M) and NHS (0.005 M) were mixed into the buffer and reacted for 3 h with stir. Thirdly, silk fibroin powder was added into the solution (10 mg mL^{-1}). After 24 h PET sheets coated with SF were taken out of the solution and dried at room temperature, which were named PET–EDC–SF group. Besides, PET sheets were immersed in MES buffer (pH = 5.5) for 2 h and then silk fibroin powder was added into the solution (10 mg mL^{-1}) without the addition of EDC and NHS, named PET–SF group. The control group was processed by the same procedures except the addition of silk fibroin powder, named PET group.

PET sheets (Fig. 1a) with porosity of 73.4 ± 3.2% (274.0 ± 13.1 g mm^{-2}) were tailored into 8 × 8 mm^2 for cell culture. As for animal experiment, they were rolled into cylindrical grafts that were 6 cm in length and 2 mm in diameter. All sheets for cell culture and grafts for animal implantation were immersed in 75% ethanol for 30 min and then irradiated by ultraviolet for 20 min. They were dried on the ventilated clean bench after the sterilizing process.

2.2 Characterization of PET–EDC–SF sheets

The surface morphology of PET and PET–EDC–SF samples was observed by scanning electron microscope (SEM; S-4800; Hitachi) at 10 kV accelerating voltage. Surface wettability was characterized by static water contact angle measurement (JC2000C1; Zhongchen Co., Ltd.). The Fourier transformation infrared (FT-IR) spectra was recorded on a Nicolet 6700 FT-IR spectrometer by the accumulation of 32 scans with a resolution of 4 cm^{-1} and a spectral range of 4000–400 cm^{-1}. The thermogravimetric analysis (TGA) was performed to measure the quantity of SF coated on PET using Linseis STA PT1600 instrument. The samples were heated from 25 to 600 °C at a heating rate of 10 °C min^{-1}. The TGA was carried out in nitrogen with the flow rate of 4 L min^{-1}. Based on the change in weight at different temperatures, the quantity of SF in the PET–EDC–SF group and the PET–SF group was calculated respectively. Samples with a length of 5 cm and a sectional area of 0.12 mm^2 were applied to measure the tensile strength by an electronic universal testing machine (CXT-4104, MTS Systems Corporation, Eden Prairie, MN, USA). The strain rate and gage length in the measurements were 5 mm min^{-1} and 30 mm. Furthermore, SEM was used to observe the SF coating morphology after mechanical analysis.

After vacuum drying, 20 ± 10 mg samples were incubated at 37 °C in a 5 mL of PBS (pH = 7.4). PBS solution was replaced freshly every 24 h and samples were weighed after being washing with distilled water for 6 times (each for 60 s), dehydrating in air for 12 h and drying in oven at 60 °C for 1 h. The percentage of weight loss of PET–EDC–SF sheets after different period of degradation was calculated using the formula: $L = (W_0$

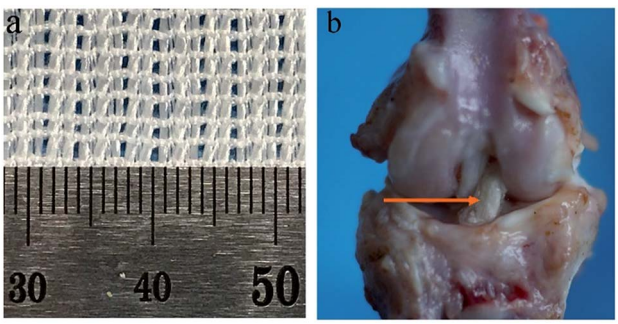

Fig. 1 (a) Gross view of PET sheets. (b) The femur-graft-tibia complex harvested 12 weeks after a surgery, red arrow pointed to PET ligament.

$- W_1)/W_0$, where L represents weight loss, W_0 represents the initial weight of the sample (mg) and W_1 represents the final weight of the sample (mg). The time points were set as 1 d, 3 d, 5 d and 7 d, respectively. The degradation rate was evaluated by calculating the slope of each time period.

2.3 Culture of BMSCs on PET–EDC–SF sheets

BMSCs were isolated from the femurs of SD rats aged 8 weeks and cultured in Dulbecco's Modified Eagle's Medium (DMEM, Invitrogen) supplemented with 10% fetal bovine serum (Invitrogen) at 37 °C with 5% CO_2 in an incubator. 0.25% trypsin was added for a 1 : 2 passage when cell density reached 80%. The PET and PET–EDC–SF sheets were placed in the bottom of 24-well plates and dipped in 500 μL complete medium for 30 min. The complete medium was removed prior to cell seeding. The BMSCs at passage three were collected by trypsin digestion method. The cell density was adjusted by adding complete medium into the cell suspension. Cell counting was performed after trypan blue staining in order to obtain a cell density of 1×10^5/mL. 500 μL cell suspension was added into each well with one sheet at the bottom. After 24 h of cell culture the sheets were transferred into another 24-well plate, followed by adding 500 μL complete medium in each well. Medium was renewed every 2 days thereafter.

After culture for 7 d, the sheets were fixed by 2.5% glutaraldehyde 2 h and followed by dehydration with graded ethanol and observed by field-emission scanning electron microscopy (FESEM; Ultra55). The sheets were sputtered with gold for 180 s at a current of 10 mA. The accelerating voltage was 20 kV and the magnifications were 500× and 1000×.

Cell counting was performed using CCK-8 assay at different time points (1, 3, 5, and 7 days) ($n = 3$). 50 μL CCK-8 solution (Dojindo, Tokyo, Kumamoto, Japan) was added into each well and reacted for 4 h in the incubator. 100 μL of supernatants were transferred to a 96-well plate and measured at 450 nm with a microplate reader (MultiSkan FC; Waltham, MA, USA). The standard curve was established according to the instruction of the kit to calculate the corresponding cell number of each specimen.

The differentiation performance at 3 and 7 d was investigated at the mRNA level by real-time PCR. Total RNA was extracted by Trizol reagent (Invitrogen) and converted to cDNA with M-MLV and reverse transcription primer OlogdT18. Reverse and forward primers for target genes (BMP2, OCN, collagen I) and housekeeping gene (Beta actin) were listed in Table 1. The 20 μL PCR reaction system contained 10 μL SYBR Premix Ex Taq, 0.2 μL primer (20 μmol L^{-1}), 2 μL cDNA template, and dH_2O. The system reaction was conducted under the following conditions: 95 °C for 5 min, followed by 42 cycles of amplification, consisting of a denaturation step at 58 °C for 10 s and an extension step at 72 °C for 10 s. The experiment was done in quintuplicate. The expression of target genes was normalized against Beta actin. Relative gene expression values were calculated by $2^{\Delta\Delta C_t}$ method.

Furthermore, the differentiation performance at 3 and 7 d was investigated at the protein level by western blot analysis. Total protein was extracted from cells cultured for 3 and 7 d. The concentration of the protein sample was measured by BCA protein assay (Pierce, IL, USA) in strict accordance with the manufacturer's instructions. Protein samples (10 μL per lane) were separated by 11% SDS-PAGE at 110 V for 90 min and the gel was stained with Ponceau S. The proteins were transferred to PVDF membranes using the wet transfer (400 mA, 90 min). The members were blocked in TBST containing 5% nonfat milk at room temperature for 2 hours and incubated with the primary antibodies (Santacruz, CA, USA) (anti-Beta actin, 1 : 1200; anti-BMP2, 1 : 600; anti-OCN 1 : 400; anti-collagen I, 1 : 300) at 4 °C overnight. The blots were then rinsed with TBST three times and incubated with the secondary antibody (Santacruz) (rabbit anti-mouse IgG, 1 : 3000) for 2 hours. ECL chemiluminescence substrates (Pierce) and X-ray film were used to detect the bands, and relative optical densities were analyzed with the image processing software (Totallab V1.10). The experiment was done in quintuplicate. Relative contents of proteins were calculated by dividing the optical density of the target band with the optical density of the beta-actin band.

2.4 Animal experiment

All animal experiment procedures were approved by the Animal Research Committee of Shanghai Jiaotong University Animal Science Department. All procedures were performed following the Guide for the Care and Use of Laboratory Animals of the National Institutes of Health and the Animal Welfare Act. Forty-six mature male New Zealand rabbits (average weight 2.8 ± 0.5 kg) underwent an ACL reconstruction procedure randomly divided into two groups: PET group and PET–EDC–SF group. Anesthesia was induced by 3% pentobarbital (30 mg kg^{-1}). After disinfection and incision along the medial border of the patella,

Table 1 Premiers for RT-PCR analysis

Accession number	Gene	Sequence
NM_017178.1	BMP2	F: 5′-AAAGCGTCAAGCCAAACACAAACA-3′ R: 5′-GAGGGGCCACGATCCAGTCAT-3′
NM_013414.1	OCN	F: 5′-ACTCCGGCGCTACCTCAACAATG-3′ R: 5′-TGGTCCGCTAGCTCGTCACAAT-3′
NM_053304.1	Collagen I	F: 5′-TCCTGACGCATGGCCAAGAAGACA-3′ R: 5′-ACAGCACTCGCCCTCCCGTTTTTG-3′
NM_031144.3	Beta actin	F: 5′-AACCCTAAGGCCAACCGTGAAAAG-3′ R: 5′-CGACCAGAGGCATACAGGGACAAC-3′

the patella was pushed to the lateral to expose the native ACL, then remove the ACL from the anatomical insertion sites. A 2 millimeter-diameter bone tunnel was drilled in the femoral and tibial insertion sites of the ACL. The PET–EDC–SF graft or PET-graft was pulled into one randomly chosen leg as the experimental group or control group. It was sutured with adjacent periosteum and soft tissue around the tunnel entrance. The wound was washed with normal saline and closed layer by layer. The animals were returned to their cages without immobilization. Ten rabbits in each group were sacrificed 6 weeks postoperatively and thirteen rabbits in each group 12 weeks postoperatively.

2.5 Histological examination

The femur-graft-tibia complexes (Fig. 1b) were harvested in each group ($n = 5$) 6 and 12 weeks after surgery respectively and fixed in 10% formalin for 48 h. Then they are embedded in a methylmethacrylate compound for the histological analysis of the graft–bone interface. The samples were sectioned with a thickness of 5 μm perpendicularly to the longitudinal axis of the tibial tunnel using a microtome (SM2500; Leica, Nussloch, Germany). These sections were stained with hematoxylin and eosin (H&E). Masson trichrome stain was performed for the sections at the time point of 12 weeks postoperatively. All of the images were visualized using inverted light microscopy (IX71SBF-2, Olympus Co., Japan) and recorded using a DP Manager (Olympus Optical Co., Japan). Histomorphometric analysis was performed based on the results of H&E staining. Three sections taken at the middle portion of the bone tunnel were adopted and each section was divided into 4 quadrants in which the interface width was measured refereed to the distance between the edge of the bone tunnel and the outer graft under 200× magnification. The average interface width for each specimen was determined by a total of 12 measurements. The investigator who performed the histomorphometric analysis was blinded to the group to which the specimen belonged.

2.6 Mechanical testing

The femur-graft-tibia complexes were harvested in each group ($n = 5$) 6 and 12 weeks postoperatively and prepared for mechanical test. All scar tissue and sutures need removing from the bone tunnel exits before fixing the complexes on the Instron machine (8874; Instron Co., Norwood, MA, USA). The femoral bone and tibial bone were immobilized firmly by clamps vertically. After being fixed firmly, the samples were preloaded with a static preload of 1 N for 5 minutes followed by loading with an elongation of 2 mm min^{-1} until the graft was ruptured or pulled out of the bone tunnel. The ultimate failure load and the stiffness were recorded.

2.7 Micro-CT analysis

The femur-graft-tibia complexes were harvested in each group ($n = 3$) 12 weeks after surgery respectively and fixed in 10% formalin for 48 h. Skyscan 1176 micro-CT imaging system (Bruker, Kontich, Belgium) was utilized to perform micro-computed tomography (micro-CT) analysis with three-dimensional reconstructions at a spatial resolution of 18 μm (1 mm aluminum filter, 65 kV, 378 μA). NRecon, Data Viewer, and CTvox (SkyScan) were performed to analyse the data. Two sections at proximal and distal femoral bone tunnel and two sections at proximal and distal tibial bone tunnel were chosen to measure the bone tunnel area respectively with ImageJ software (National Institutes of Health, USA). The investigator who performed the micro-CT data analysis was blinded to the group to which the specimen belonged.

2.8 Statistic analysis

The mean and standard deviation were used to describe the data, and the data analysis was performed using the Stata10.0 software (Stata Corp, USA). Comparison of the quantitative results were carried out using a Student's *t*-test. All *P*-value were two-sided and the statistical significance level was set to 0.05.

3. Results

3.1 Characterization of sheets

SEM observations of PET sheets and PET–EDC–SF sheets were shown in Fig. 2a and b. The surface of PET was wrapped by a layer of rugged film after the application of SF coating, which is originally smooth. In the water contact angle tests, the droplet of water adhered on the surface of pure PET stably but penetrated into sheets of PET–EDC–SF quickly. Dynamic contact angle measurement was utilized and the image was chosen to measure the transient contact angle 0.4 s after 5 μL water

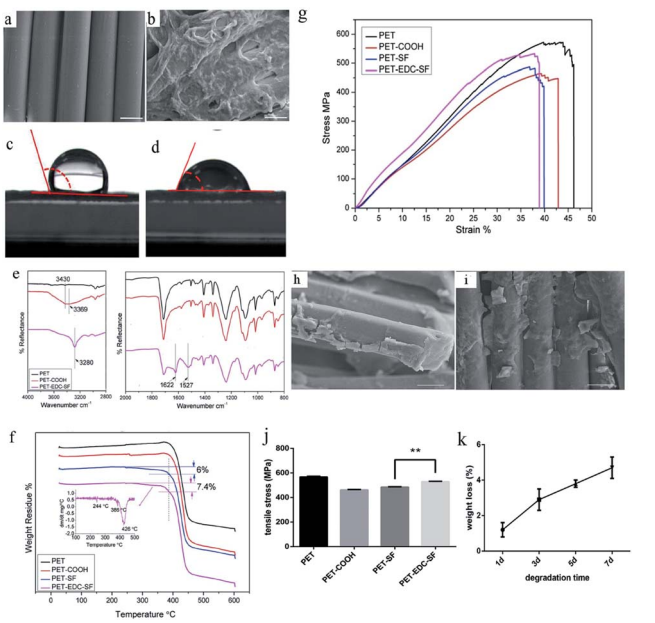

Fig. 2 SEM morphology of PET (a) and PET–EDC–SF (b), bar = 10 μm. Water contact angle image of PET (c) and PET–EDC–SF (d). FTIR (e) of PET, PET–COOH, PET–SF and PET–EDC–SF. TG curves (f) of PET, PET–COOH, PET–SF and PET–EDC–SF. Mechanical test of PET, PET–COOH, PET–SF and PET–EDC–SF (g, j). SF morphology in the PET–SF group (h) and PET–EDC–SF group (i) after mechanical test. Bar = 10 μm. The degradation rate of PET–EDC–SF group (k).

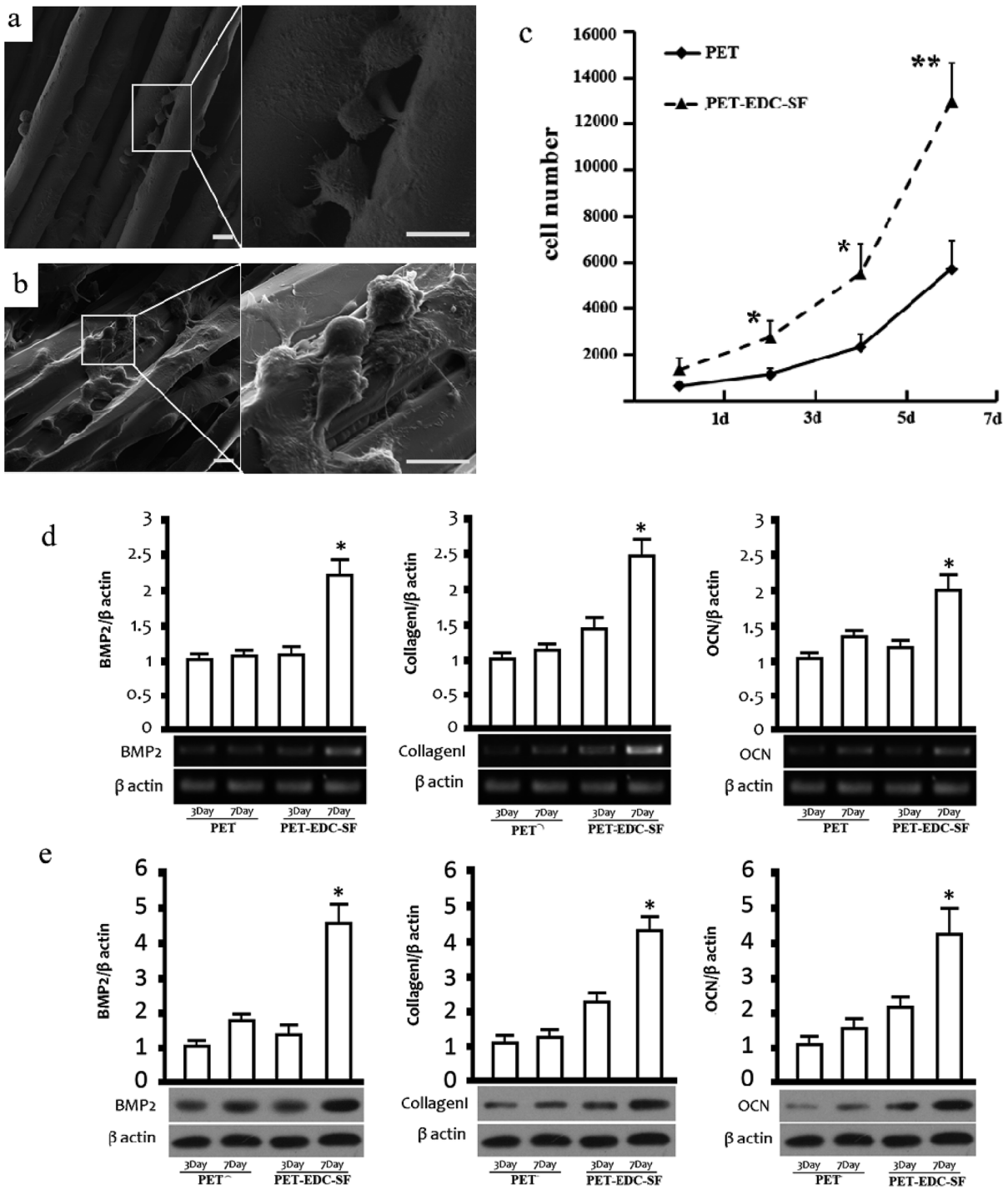

Fig. 3 Scanning electron micrographs of BMSCs cultured on PET (a) and PET–SDC–SF (b) for 7 days. Bar = 10 μm. (c) Proliferation of BMSCs of PET group and PET-SF group by CCK-8 assay. (d) Gene expression level of BMP-2, collagen I and OCN relative to beta actin in BMSCs cultured for 3 and 7 d in PET group and PET–SF group by real-time PCR analysis. The upper histograms showed C_t value calculated by $2^{\Delta\Delta C_t}$ method, the lower images were PCR production electrophoretogram. (e) Protein expression level of BMP-2, collagen I and OCN relative to beta actin in BMSCs cultures for 3 and 7 d in PET group and PET–SF group by western blot analysis. The upper histograms showed optical density results, the lower images showed the target bands. *$p < 0.05$, **$p < 0.01$.

dropped on the surface of PET–EDC–SF sheets. The contact angle decreased from 106° to 58.5° after the application of SF coating (Fig. 1c and d). Increase of surface roughness and improvement of hydrophilicity were acquired by using SF coating. FTIR was used to detect the SF secondary structure. In Fig. 2e, the broad and strong peak at 3369 cm^{-1} (assigned to –OH vibration) exhibited after PET was boiled in NaOH aqueous solution, which demonstrated that carboxyl groups on the

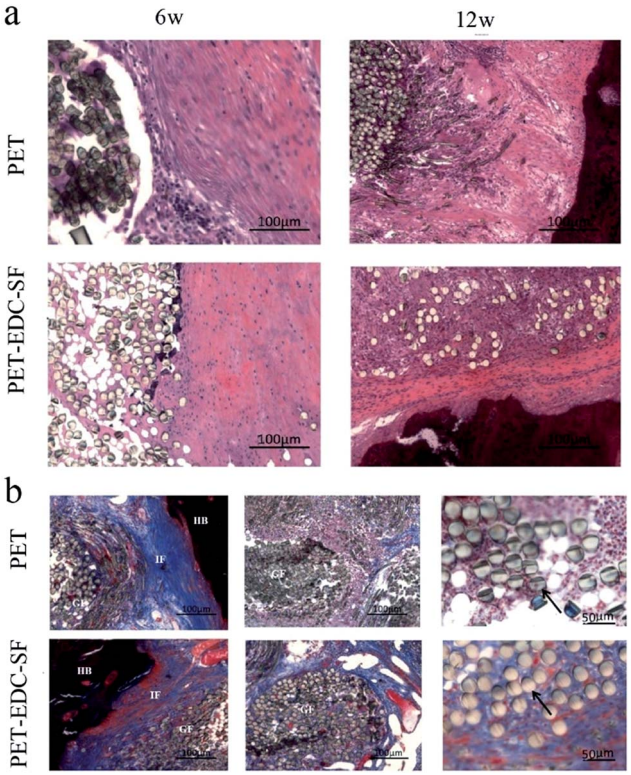

Fig. 4 (a) H&E staining results of PET group and PET–EDC–SF group. (b) Masson staining results of PET group and PET–EDC–SF group 12 weeks after surgery (HB, host bone; IF, interface; GF, graft; black arrow pointing to PET fiber).

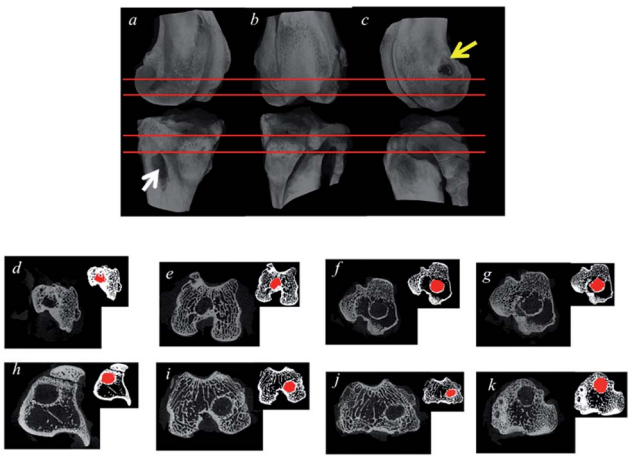

Fig. 5 3D views from the front (a) and two sides (b and c), the white arrow pointing to the tibial aperture of bone tunnel and the yellow arrow pointing to the femoral aperture of bone tunnel, red lines illustrated the positions of four sections in a sample. Four sections randomly cut out from one sample in the PET–EDC–SF group (d–g) and in the PET group (h–k) to measure the cross sectional area of bone tunnel (marked with the red color), two sections from tibia and two section from femur.

surface of PET were exposed. The peak at 3280 cm^{-1} exhibited after SF coating was attributed to hydrogen bond of SF. The characteristic peak 1527 cm^{-1} in amide II region and 1622 cm^{-1} in amide I region verified the SF β-sheet structure. Thermal characteristics (Fig. 2f) showed the weight loss at 386 °C and 426 °C was due to the decomposition of PET and the weight loss at 244 °C was due to the decomposition of SF.[24,25] The quantity of SF in the PET–EDC–SF group and the PET–SF group were 7.4% and 6%. As shown in Fig. 2g, after being boiled in NaOH aqueous solution, PET samples exhibited a decline in tensile strength. However, the tensile strength of the PET–EDC–SF group 528.3 ± 3.51 MPa was higher than that of the PET–SF group 484.0 ± 3.61 MPa ($P < 0.01$) (Fig. 2j). Besides, SF coating on both the PET–SF group and the PET–EDC–SF group exhibited cracks after mechanical testing (Fig. 2h). The remaining SF in the PET–EDC–SF group was more than that in the PET–SF group. After incubated in PBS, the weight loss of samples increased with exposure time (Fig. 2k). After 7 d, the weight loss of the scaffolds incubated in PBS is about 4.7%.

3.2 Proliferation, differentiation of BMSCs on PET sheets

The scanning electron micrographs (Fig. 3a and b) showed that the majority of cells in both group had circular shapes. The cells cultured for 7 days in the PET–EDC–SF group exhibited polygon and spindle shape. Filopodia were obviously observed in the PET–EDC–SF group through which cells adhered on the substrate. Besides, the extracellular matrix secretion was promoted in the PET–EDC–SF group.

As shown in Fig. 3c, the CCK-8 results revealed that the BMSCs proliferated with time on both group of the sheets. The cells in the PET–EDC–SF group exhibited a higher proliferation level than those in the PET group after cultivation of 1, 3, 5 and 7 days. The different proliferation levels have statistical significance except the result of culture for 1 day. The mRNA and protein expression levels of BMP-2, collagen I and OCN were measured quantitatively by RT-PCR and western blot respectively (Fig. 3d and e). After culture for 3 days, the BMP-2, collagen I and OCN mRNA level between PET group and PET–EDC–SF group exhibited no significant difference. After culture for 7 days, BMP-2, collagen I and OCN mRNA level in the PET–EDC–SF group were obviously upregulated compared with the PET group. Furthermore, the protein expression level of three targeted genes showed the same trend with the mRNA expression level.

3.3 *In vivo* osseointegration findings

The histological results of H&E staining were shown in Fig. 4a. There was a sharp dividing line between PET fibers and self-tissue in the PET group 6 weeks after surgery. In the PET–EDC–SF group self-tissue was penetrating to PET fibers. At 12 weeks, graft and bone contacted closely and PET fibers were encircled by self-tissue in the PET–EDC–SF group. However, thick fibrous tissue exhibited at the interface of the PET group.

The Masson staining results (Fig. 4b) indicated the same process. There were a mass of inflammatory cells around the PET fibers in the PET group 12 weeks after surgery, meanwhile the PET fibers in PET–EDC–SF group were almost encircled by collagen.

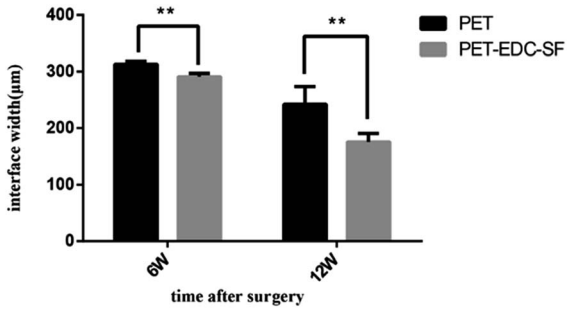

Fig. 6 Quantitative analysis of graft–bone interface width. *$P < 0.05$, **$P < 0.01$.

Micro-CT images were shown in Fig. 5. The average cross sectional area of bone tunnel in the PET–EDC–SF group was smaller than that in the PET group, but there was no significant difference between the two groups (3.254 ± 0.128 cm^2 *vs.* 4.250 ± 0.507 cm^2, $P > 0.05$).

Histomorphometric analysis (Fig. 6) showed that the graft–bone interface width in the PET–EDC–SF group was smaller than those in the PET group at the 6th week (291.00 ± 6.24 μm *vs.* 313.20 ± 5.45 μm, $P < 0.01$) and 12th week (175.40 ± 14.94 μm *vs.* 242.20 ± 31.61 μm, $P < 0.01$) after surgery.

3.4 Mechanical testing

No graft ruptured in the mechanical analysis and all samples were pulled out from the bone tunnel. The mechanical results were showed in Fig. 7a and b. The failure loads of PET group and PET–EDC–SF group were almost equal at 6 weeks post-operatively (46.00 ± 4.08 N *vs.* 46.60 ± 4.16 N, $P = 0.0833$). At the 12th week, the failure load of PET–EDC–SF group was higher than that of the PET group, but still no significant difference between the two groups (66.02 ± 6.08 N *vs.* 70.05 ± 6.48 N, $P = 0.0801$). There was no statistically significant difference in the stiffness value between the PET group and PET–EDC–SF group at two time points (4.39 ± 0.30 N mm^{-1} *vs.* 4.77 ± 0.61 N mm^{-1}, $P = 0.1737$; 6.23 ± 0.78 N mm^{-1} *vs.* 6.46 ± 0.83 N mm^{-1}, $P = 0.1227$).

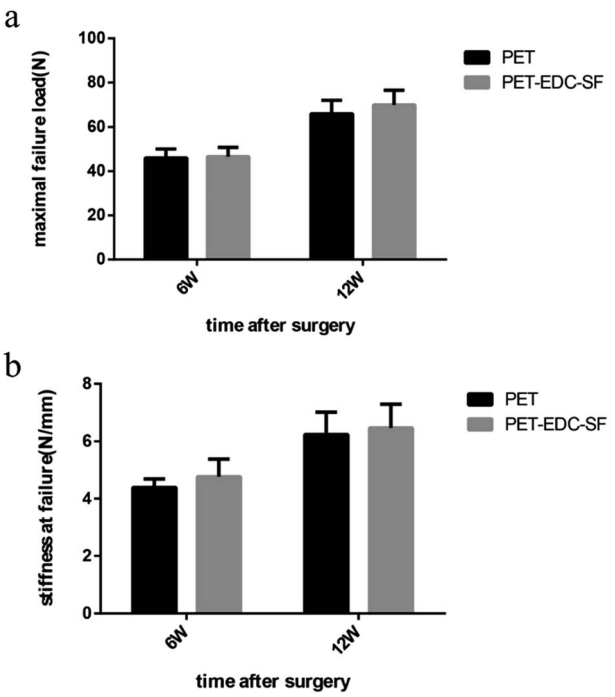

Fig. 7 Mechanical examinations for graft-bone healing. Comparison of maximal failure load (a) and stiffness (b) of PET group and PET–SF group. *$P < 0.05$, **$P < 0.01$.

4. Discussion

The selection of ACL grafts is a quite controversial issue for ACL reconstruction under arthroscopy around the world.[26,27] Artificial ligament made of PET material is in the spotlight owing to its good clinical follow-up outcomes.[28,29] In spite of the insufficiency of long-term follow-up results, it is acknowledged that the PET ligament is the optimal choice of synthetic ligament at present. However, PET is a hydrophobic material short of osteoinduction and osteoconduction, leading to the disadvantage of the required graft-bone healing. Surface modification is an effective method to cover this shortage, thus enhance graft-bone healing and achieve good clinical outcome. SF has been extensively studied in bone tissue engineering for its good biocompatibility. Pure SF scaffolds and SF structures seeded with various types of cells including BMSCs, chondrocytes, and osteoblasts have been investigated in order to obtain bone or ligament more close to native structure,[8,15] but the mechanical strength of the tissue based on SF scaffold was not durable and stable. In this study, we combined the good biocompatibility of SF and persistent mechanical strength of PET together. SF was used to modify the PET ligaments in the form of coating aimed to provide a convenient and efficient method to enhance osseointegration of PET ligaments.

The ideal coating can ameliorate the biocompatibility of substrate material with firm adhesion.[30] Hu *et al.* had proved that higher surface roughness and stronger micro/nano-scale surface patterns of silk-tropoelastin biomaterials enhanced the proliferation and osteogenic-differentiation of hMSCs.[31] In present study, the surface roughness was increased after SF coating according to the SEM observation, which was supposed to benefit osteogenic-differentiation of BMSCs *in vitro*. The FTIR spectra proved that SF was immobilized onto PET *via* EDC/NHS crosslinking method. Besides, the decrease of water contact angle indicated the improvement of hydrophilicity, which is beneficial to cell growth and attachment.[32] Quantity of SF coated on PET also could affect its biological performance *in vivo* and a requirement for efficient biological functionality of SF is that SF coating must adhere satisfactorily to the underlying substrate. TGA results proved that the quantity of SF coated on PET *via* EDC–NHS was more than that *via* dip coating in this study. Jiang *et al.*[18] pretreated PET with plasma surface modification and then coated PET with SF through dip coating, but the quantity of SF was not measured. The results of SEM suggested the quantity of SF coated on PET in our study was more than that in Jiang's study. On the other, the tensile

strength of PET–EDC–SF group was higher than the PET–SF group which demonstrated that EDC–NHS crosslink had a positive effect on the mechanical property of PET. The remaining SF in the PET–EDC–SF group after mechanical test was more than the PET–SF group, which suggested the bonding strength *via* EDC–NHS was superior to that *via* dip coating. Higher bonding strength could avoid delamination and thus provide a stable function while the coating material integrates with host bone tissue.[33] Liang *et al.*[34] immobilized SF onto PET film *via* two different methods: plasma pretreatment followed by SF dip coating and plasma-induced acrylic acid graft polymerization and subsequent covalent immobilization of SF on PET film. Both were proved to promote the cytocompatibility of PET effectively. However, the bonding strength test and TGA was not performed in Liang's study, a direct comparison analysis on bonding strength and quantity of SF coating *via* different coating methods cannot be conducted. According to our results, EDC–NHS crosslink was a superior coating method compared with dip coating for it increased SF quantity on PET and contributed to greater bonding strength. Study of *in vitro* degradation helps to understand and predict the *in vivo* degradation behavior of the PET–EDC–SF sheets. After 7 d, the weight loss of the scaffolds incubated in PBS is about 4.7%. According to the reports of almost no weight loss of SF scaffolds in PBS,[35] the results reveal that the PET–EDC–SF sheets is stable in PBS.

In the present study, we furtherly investigated the biocompatibility of the coating. It was proved that the initial stage of osseointegration was cell migration to the surface of grafts,[36] and the first cells migrating at the graft surface were multipotent mesenchymal cells.[37] It was recognized that BMSCs were conductive to graft-bone healing and have been widely used in tissue engineering of ligaments.[38,39] Therefore, BMSCs were adopted to investigate the biocompatibility of PET sheets *in vitro* in this study. Cellular differentiation was assessed by evaluating the expression level of BMP-2, collagen I, and OCN. Osteogenic differentiation of BMSCs is one the pivotal steps to determine the success in graft-bone healing. Fei *et al.* found that BMP-2 could induce gene and protein expression of Runx2 and then regulated the expression of osteogenic-related genes such as ALP and OCN at the transcription level.[40] OCN synthesized by mature osteoblast-like cells in the ECM of bone tissue is an important indicator of the osteogenic differentiation.[41] It was suggested that the stimulation of the expression of osteogenic gene OCN was related to the upregulation of BMP-2 by SF coating in this study. Besides, BMP-2 is the main driving force of osteogenic process because it can induce more BMP-2 secretion *via* autocrine and paracrine.[42] Consequently, collagen I protein as the major organic component of nature bone was accumulated more in the PET–EDC–SF group. Lee *et al.* cultured rabbit BMSCs on SF/β-TCP scaffolds of each different ratios of SF and β-TCP (100 : 0, 75 : 25, 50 : 50, 25 : 75) and found that ALP activity of BMSCs increased in pure SF scaffold more than other groups.[43] Despite SF was not fabricated as a scaffold in this study, we found that SF in the form of coating still helped the differentiation of BMSCs. These results indicated SF coating facilitated the cytocompatibility of PET material.

Moreover, the *in vivo* histological findings revealed the positive impact of SF coating onto graft-bone healing. It was recognized that osseointegration was of great significance for ACL reconstruction under arthroscopy using synthetic ligament. On one hand, osteolysis widening of bone tunnel is a concern for long term use of artificial ligament. Muren *et al.* performed a 13–15 year follow-up study of Gore-Tex ACL graft and reported that most of the non-ruptured implants resulted in tunnel widening.[44] On the other, integration into the host bone helps to biomechanically stabilize the implant and to reduce or eliminate wear particles caused by excessive friction between the artificial implant and the surrounding hard issues.[45] New born tissues penetrated into the PET ligaments in the PET–EDC–SF group 12 weeks postoperatively, while a large amount of inflammatory cells were observed around the PET fibers in the PET group. The graft–bone interface width of PET–EDC–SF group was smaller, indicating the osteointegrating performance of PET material was improved by SF coating. There are three successive phases in the ligamentization process of autografts and allografts including early healing phase, intense remolding phase, and maturation phase and a structure similar to native ACL is obtained as a result of the corresponding pathophysiologic changes during each phase.[46] Despite the ligamentization process of synthetic implants is still unclear, it is indicated earlier graft-bone healing leads to better surgery outcome.[47] Wang *et al.* incorporated HAP nano-particles into silk matrix in rabbit radial segmental bone defect model and observed bone regeneration within 8 weeks.[48] Kweon *et al.* found the same results in rabbit bilateral parietal bony defect model.[49] 12 weeks postoperatively the cross sectional bone tunnel area based on micro-CT results in the PET–EDC–SF group was smaller despite the differences were not statistically significant, suggesting that silk coating facilitates bone regeneration within 12 weeks. Therefore, SF coating could help to ensure a good ligamentization process for ACL reconstruction using PET ligaments.

Despite enhanced histological graft–bone contact was observed at 12th week after operation in the present study, a significant biomechanical improvement when performing pull-out tests was not observed. Vaquette *et al.* modified the surface of PET ligament with polystyrene sodium sulfonate (PolyNaSS) and implanted the grafted ligament in an ovine model for ACL reconstruction. Likewise, no biomechanical differences in pull-out loads were found at 1 year post-implantation.[45] Using an alternate soaking processing solutions containing phosphate or calcium ions, Mutsuzaki *et al.* designed a CaP-hybridised tendon for ACL reconstruction in goat and the pull-out test results were not significantly different between the CaP group and the control group.[50,51] Furthermore, they analyzed knee kinematics and *in situ* force using a robotic testing system simulator. The *in situ* force in the graft in response to a 50 N anteroposteriortibial load at different knee flexion angles including full extension, 60° and 90° of flexion was investigated in a goat model at 1 year postoperatively. The result of the CaP group was close to that of native ligament whereas the control graft reached only 50% of this value.[52] Together with our mechanical results, all of these observations

indicated that the enhanced integration in the bone tunnel might not be equal to higher pull out load. Actually, ultimate failure load measured by pull-out test is a common index for determining graft-bone healing, but not a comprehensive measurement of biomechanical behaviors. Biomechanical testing techniques simulating more closely to realistic load condition are conductive to improve clinical relevance of animal experiments.

There are some limitations in this study. We merely proved that SF coating *via* EDC/NHS crosslink enhanced the osseointegration of PET ligaments, however we have not dig into the cellular and molecular mechanisms thoroughly. Regarding to the animal model, the time points were set at 6 weeks and 12 weeks, longer-time observation was needed in consideration of the biodegradation of silk fibroin. Besides, the simple pull-out biomechanical tests were not comprehensive enough to measure the biomechanical behaviors.

5. Conclusions

This study verified the positive effect of SF coating onto PET ligament for ACL reconstruction. (1) SF could be utilized to modify PET material *via* EDC/NHS crossslinking method; (2) higher proliferation level and upregulated BMP-2, OCN, collagen I expression of BMSCs in the experimental group proved that SF coating was efficient to enhance the osseointegration of PET; (3) improved osseointegration within the bone tunnel in the rabbit ACL reconstruction *in vivo* suggested that SF can be used as a versatile biomaterial in a complementary approach to prepare a synthetic ligament in possession of both strong mechanical properties and good biocompatibility.

Conflicts of interest

The authors declared no conflict of interests.

Acknowledgements

This work was supported by National 863 Hi-tech Project (2015AA033703); National Natural Science Foundation of China (NO. 51503153, NO. 81370052 and NO. 81572108); National Key R&D Program of China (2016YFC1100300); the Shanghai Rising-Star Program (15QB1402100).

References

1 B. A. Levy, *N. Engl. J. Med.*, 2010, **363**, 386–388.
2 R. B. Frobell, E. M. Roos, H. P. Roos, J. Ranstam and L. S. Lohmander, *N. Engl. J. Med.*, 2010, **363**, 331–342.
3 P. Ranger, A. Renaud, P. Phan, P. Dahan, E. De Oliveira Jr and J. Delisle, *Int. Orthop.*, 2011, **35**, 1477–1482.
4 X. Pan, H. Wen, L. Wang and T. Ge, *Eur. J. Orthop. Surg. Traumatol.*, 2013, **23**, 819–823.
5 F. Hamido, A. K. Misfer, H. Al Harran, T. A. Khadrawe, A. Soliman, A. Talaat, A. Awad and S. Khairat, *Knee*, 2011, **18**, 373–378.
6 K. Gao, S. Chen, L. Wang, W. Zhang, Y. Kang, Q. Dong, H. Zhou and L. Li, *Arthroscopy*, 2010, **26**, 515–523.
7 G. H. Altman, F. Diaz, C. Jakuba, T. Calabro, R. L. Horan, J. Chen, H. Lu, J. Richmond and D. L. Kaplan, *Biomaterials*, 2003, **24**, 401–416.
8 B. Kundu, R. Rajkhowa, S. C. Kundu and X. Wang, *Adv. Drug Delivery Rev.*, 2013, **65**, 457–470.
9 K. Chen, P. Shi, T. K. Teh, S. L. Toh and J. Goh, *J. Tissue Eng. Regener. Med.*, 2016, **10**, 284–293.
10 N. M. Yudintceva, Y. A. Nashchekina, M. I. Blinova, N. V. Orlova, A. N. Muraviov, T. I. Vinogradova, M. G. Sheykhov, E. Y. Shapkova, D. V. Emeljannikov, P. K. Yablonskii, I. A. Samusenko, A. L. Mikhrina, A. V. Pakhomov and M. A. Shevtsov, *Int. J. Nanomed.*, 2016, **11**, 4521–4533.
11 X. F. Shen, Y. X. Zhang, Y. Gu, Y. Xu, Y. Liu, B. Li and L. Chen, *Biomaterials*, 2016, **106**, 205–216.
12 S. Fare, P. Torricelli, G. Giavaresi, S. Bertoldi, A. Alessandrino, T. Villa, M. Fini, M. C. Tanzi and G. Freddi, *Mater. Sci. Eng., C*, 2013, **33**, 3601–3608.
13 H. Fan, H. Liu, S. L. Toh and J. C. Goh, *Biomaterials*, 2009, **30**, 4967–4977.
14 A. Teuschl, P. Heimel, S. Nurnberger, M. van Griensven, H. Redl and T. Nau, *Am. J. Sports Med.*, 2016, **44**, 1547–1557.
15 H. G. Li, J. B. Fan, L. G. Sun, X. C. Liu, P. Z. Cheng and H. B. Fan, *Biomaterials*, 2016, **106**, 180–192.
16 R. D. Abbott, E. P. Kimmerling, D. M. Cairns and D. L. Kaplan, *ACS Appl. Mater. Interfaces*, 2016, **8**, 21861–21868.
17 H. Li, S. Chen, J. Chen, J. Chang, M. Xu, Y. Sun and C. Wu, *ACS Appl. Mater. Interfaces*, 2015, **7**, 14708–14719.
18 J. Jiang, F. Wan, J. J. Yang, W. Hao, Y. X. Wang, J. R. Yao, Z. Z. Shao, P. Zhang, J. Chen, L. Zhou and S. Y. Chen, *Int. J. Nanomed.*, 2014, **9**, 4569–4580.
19 Y. Wang, X. Wang, J. Shang, H. Liu, Y. Yuan, Y. Guo, B. Huang and Y. Zhou, *Eur. Spine J.*, 2016, 1–10.
20 D. V. Bax, N. Davidenko, D. Gullberg, S. W. Hamaia, R. W. Farndale, S. M. Best and R. E. Cameron, *Acta Biomater.*, 2017, **49**, 218–234.
21 J. C. Ashworth, M. Mehr, P. G. Buxton, S. M. Best and R. E. Cameron, *Adv. Healthcare Mater.*, 2015, **4**, 1317–1321.
22 J. Zhou, B. Zhang, L. Shi, J. Zhong, J. Zhu, J. Yan, P. Wang, C. Cao and D. He, *ACS Appl. Mater. Interfaces*, 2014, **6**, 21813–21821.
23 F. Everaerts, M. Torrianni and M. Hendriks, *J. Biomed. Mater. Res., Part A*, 2008, **85**, 547–555.
24 M. P. Gashti, S. Moradian, A. Rashidi and M.-E. Yazdanshenas, *Polym. Polym. Compos.*, 2015, **23**, 285.
25 S. Prasong, S. Wilaiwan and K. Nualchai, *Int. J. Chem. Technol.*, 2010, **1**, 21–27.
26 C. R. Bottoni, E. L. Smith, J. Shaha, S. S. Shaha, S. G. Raybin, J. M. Tokish and D. J. Rowles, *Am. J. Sports Med.*, 2015, **43**, 2501–2509.
27 K. E. Webster, J. A. Feller, N. Hartnett, W. B. Leigh and A. K. Richmond, *Am. J. Sports Med.*, 2016, **44**, 83–90.

28 L. M. Batty, C. J. Norsworthy, N. J. Lash, J. Wasiak, A. K. Richmond and J. A. Feller, *Arthroscopy*, 2015, **31**, 957–968.
29 J. H. Lubowitz, *Arthroscopy*, 2015, **31**, 969–970.
30 A. E. Nel, L. Madler, D. Velegol, T. Xia, E. M. Hoek, P. Somasundaran, F. Klaessig, V. Castranova and M. Thompson, *Nat. Mater.*, 2009, **8**, 543–557.
31 X. Hu, S. H. Park, E. S. Gil, X. X. Xia, A. S. Weiss and D. L. Kaplan, *Biomaterials*, 2011, **32**, 8979–8989.
32 J. Jiang, C. Ai, Z. Zhan, P. Zhang, F. Wan, J. Chen, W. Hao, Y. Wang, J. Yao, Z. Shao, T. Chen, L. Zhou and S. Chen, *Artif. Organs*, 2016, **40**, 385–393.
33 C. Wu, Z. Chen, Q. Wu, D. Yi, T. Friis, X. Zheng, J. Chang, X. Jiang and Y. Xiao, *Biomaterials*, 2015, **71**, 35–47.
34 M. Liang, J. Yao, X. Chen, L. Huang and Z. Shao, *Mater. Sci. Eng., C*, 2013, **33**, 1409–1416.
35 B. B. Mandal and S. C. Kundu, *Acta Biomater.*, 2010, **6**, 360–371.
36 W. Singhatanadgit, *Bone Tissue Regener. Insights*, 2012, **2**, 1–11.
37 Z. Schwartz, J. Y. Martin, D. D. Dean, J. Simpson, D. L. Cochran and B. D. Boyan, *J. Biomed. Mater. Res.*, 1996, **30**, 145–155.
38 H. Li, J. Fan, L. Sun, X. Liu, P. Cheng and H. Fan, *Biomaterials*, 2016, **106**, 180.
39 N. L. Leong, F. A. Petrigliano and D. R. Mcallister, *J. Biomed. Mater. Res., Part A*, 2014, **102**, 1614.
40 L. Fei, C. Wang, Y. Xue, K. Lin, J. Chang and J. Sun, *J. Biomed. Mater. Res., Part B*, 2012, **100**, 1237–1244.
41 S. A. Oh, H. Y. Lee, J. H. Lee, T. H. Kim, J. H. Jang, H. W. Kim and I. Wall, *Tissue Eng., Part A*, 2012, **18**, 1087–1100.
42 Y. D. Cho, W. J. Kim, W. J. Yoon, K. M. Woo, J. H. Baek, G. Lee, G. S. Kim and H. M. Ryoo, *J. Cell. Physiol.*, 2012, **227**, 2287–2296.
43 D. H. Lee, N. Tripathy, J. H. Shin, J. E. Song, J. G. Cha, K. D. Min, C. H. Park and G. Khang, *Int. J. Biol. Macromol.*, 2017, **95**, 14–23.
44 O. Muren, L. Dahlstedt, E. Brosjo, M. Dahlborn and N. Dalen, *Acta Orthop.*, 2005, **76**, 270–274.
45 C. Vaquette, V. Viateau, S. Guerard, F. Anagnostou, M. Manassero, D. G. Castner and V. Migonney, *Biomaterials*, 2013, **34**, 7048–7063.
46 L. Pauzenberger, S. Syre and M. Schurz, *Arthroscopy*, 2013, **29**, 1712–1721.
47 H. Li, Z. Yao, J. Jiang, Y. Hua, J. Chen, Y. Li, K. Gao and S. Chen, *Arthroscopy*, 2012, **28**, 583–586.
48 G. Wang, H. Yang, M. Li, S. Lu, X. Chen and X. Cai, *J. Bone Jt. Surg., Br. Vol.*, 2010, **92**, 320–325.
49 H. Kweon, K. G. Lee, C. H. Chae, C. Balazsi, S. K. Min, J. Y. Kim, J. Y. Choi and S. G. Kim, *J. Oral Maxillofac. Surg.*, 2011, **69**, 1578–1586.
50 H. Mutsuzaki, M. Sakane, S. Hattori, H. Kobayashi and N. Ochiai, *Biomed. Mater.*, 2009, **4**, 045013.
51 H. Mutsuzaki, M. Sakane, H. Nakajima and N. Ochiai, *Knee*, 2012, **19**, 455–460.
52 H. Mutsuzaki, M. Sakane, H. Fujie, S. Hattori, H. Kobayashi and N. Ochiai, *Am. J. Sports Med.*, 2011, **39**, 1059–1066.